THE JOURNAL OF PHYSICAL CHEMISTRY A

Article

pubs.acs.org/JPCA

Influence of the Glass Transition on Rotational Dynamics of Dyes in Thin Polymer Films: Single-Molecule and Ensemble Experiments

Beatriz Araoz,[†] Aquiles Carattino,[†,⊥] Daniela Täuber,[‡] Christian von Borczyskowski,*[,‡] and Pedro F. Aramendia*[,†,§,∥]

[†]INQUIMAE and Dept. Química Inorgánica Analítica y Química Física. Facultad de Ciencias Exactas y Naturales, Universidad de Buenos Aires, Pabellón 2, Ciudad Universitaria, C1428EHA Ciudad de Buenos Aires, Argentina

[‡]Institute of Physics and nanoMA, Technische Universität Chemnitz, 09107 Chemnitz, Germany

[§]Centro de Investigaciones en Bionanociencias, CIBION-CONICET, Godoy Cruz 2390, 1425 Ciudad de Buenos Aires, Argentina

[∥]Dept. Química Inorgánica Analítica y Química Física. Facultad de Ciencias Exactas y Naturales, Universidad de Buenos Aires, Pabellón 2, Ciudad Universitaria, C1428EHA Ciudad de Buenos Aires, Argentina

Supporting Information

ABSTRACT: We performed polarized fluorescence emission studies of Nile Red (NR) in poly(methyl methacrylate) (PMMA), poly(ethyl methacrylate) (PEMA), and poly(butyl methacrylate) (PBMA) at the single molecule (SM) and at the ensemble level to study the in cage movements of the ground-state molecule in polymer films of nanometric thickness at room temperature. Experiments were performed with wide field irradiation. At the ensemble level, the linearly polarized irradiation was used to induce a photoselection by bleaching, which is compensated by rotational diffusion. Both results show an appreciable difference in mobility of NR in the films that is correlated with the different glass-transition temperatures of the films, particularly in PEMA, which displays a clearly distinct behavior between the 200 nm films, representing a rigid environment, and the 25 nm ones, showing much higher mobility. We developed a model of broad application for polarized photobleaching that allows obtaining rotational diffusion coefficients and photobleaching quantum yields in an easy way from ensemble experiments. The parameters obtained from ensemble measurements correlate well with the results from SM experiments.

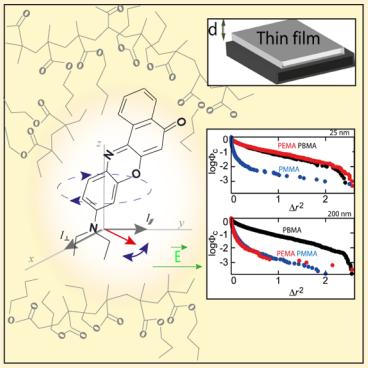

INTRODUCTION

Thin polymer films containing dye molecules are important in photoactive coatings, filters, OLEDS, and solar cells. In these applications, the interaction of the dye with the near environment, the dye−polymer cage, is crucial.[1,2]

Polymers are heterogeneous systems at the molecular level. Therefore, dye−polymer interactions can have a distribution of behaviors depending on the location of the probe and the conformation of the polymer chains around it.[3−5] The mobility of the probe in a polymer cage plays an important role in the deactivation and reactive pathways of unimolecular reactions after light absorption (isomerization, dissociation). While ensemble methods can only yield average values, single molecule (SM) experiments provide detailed information[6−8] about the distribution of singularities related to the variety of polymer environments.[9−11]

It is well known that thin polymer films have different mechanical properties compared with thick films.[12,13] Particularly below 100 nm thickness, confinement and boundary effects have a profound influence on the glass-transition temperature (T_g) of thin films.[14−16] Differences as high as 30 K compared with the bulk T_g have been measured. Therefore, it is expected that changes in T_g are accompanied by changes in the local mobility of the cage even at room temperature, influencing the dynamics of the embedded dyes. A lower T_g corresponds to environments with higher flexibility and thus will be reflected in a larger mobility.

Investigations of fluorescence emission anisotropy are widely used to monitor orientational changes in conformational rearrangements, molecular association interactions, and local mobility.[12,17,18] It is usually applied to monitor excited-state dynamics in cases where rotational diffusion takes place at a rate comparable to singlet excited state lifetime (0.1 to 100 ns in practice), but the rotational correlation time in glassy polymers under and around T_g is much longer, attaining even the time range of seconds, due to environment rigidity.[11,19−21] In this situation, the expected value of the fluorescence emission anisotropy will reflect the initial distribution of fluorophores in the sample. In the ensemble experiment, fluctuations of individual fluorophores average to zero, and thus a time-independent anisotropy value is expected, which is related to the statistical average of fluorophore orientations in the sample. The orientational fluctuations take place with the

Special Issue: Current Topics in Photochemistry

Received: January 9, 2014
Revised: May 28, 2014
Published: May 29, 2014

   dx.doi.org/10.1021/jp500272y | J. Phys. Chem. A 2014, 118, 10309−10317

characteristic rotational diffusion time of the probing dye molecules and can only be observed in SM experiments or in selected samples of a small number of molecules where correlated fluctuations are still important compared with the total signal.

Therefore, using SM fluorescence emission anisotropy, it is possible to determine sudden changes in the orientation of the dye molecules embedded in the polymer matrix, independently of their excited-state lifetime.[22,23] In fact, this type of measurement has been extensively applied for dyes in polymeric matrices to determine chain orientation[24] or the heterogeneous nature of the rotation dynamics near the polymer glass-transition temperature.[10,11,25−29] If the fluorescent molecule remains in the same orientation between absorption and emission of the photon, the emitted fluorescence will report the orientation at the moment of the absorption. As previously stated, this will be the common situation in glassy polymers. In ensemble measurements under these conditions, the emission anisotropy will be constant in time due to ensemble averaging. For an SM, on the contrary, monitoring the emission anisotropy in time provides a report of the orientational fluctuation of the molecule between successive events of excitation and thus provides information on orientational diffusion. In this way, it is possible to monitor molecular reorientation of the dye and to relate it to the different types of environments where the molecules can be found; that is, more rigid surroundings will lead to a lower frequency of rearrangements or to smaller amplitudes of them.[30,31]

Single-molecule experiments provide rich insight into the dye−polymer dynamics, but they always raise the question of the proper selection of a representative molecular ensemble. Therefore, ensemble experiments can be used as a valuable reference for this fact. Ensemble experiments are normally faster to perform and easier to analyze. In this work, we also report ensemble measurements of the same systems used for SM experiments and provide a link between the two types of experiments.

In general, photobleaching[32] causes a perturbation in rotational diffusion studies.[33,34] In this work, we propose a method to take advantage of polarized photobleaching to study rotational diffusion in polymer films under continuous irradiation. Basically, linearly polarized photobleaching is used to create an asymmetry in the orientational distribution of an ensemble of fluorescent molecules, which is partially compensated by rotational diffusion. We use a model that considers linearly polarized irradiation and photobleaching. Molecules are free to reorient isotropically in three dimensions, and each molecule emits light polarized parallel to the absorption. The resulting time-dependent linearly polarized emission components are used to build the time-dependent steady-state anisotropy.

SM measurements of emission of Nile Red in a series of poly(alkyl methacrylate) films of nanometric thickness provide evidence of the varying mobility of dye molecules in the polymer cage for different film thickness. From the mean orientation fluctuation, we derive rotational diffusion coefficients. These values are compared with rotational correlation coefficients obtained from ensemble experiments in the same systems. The latter also provide photobleaching quantum yields for ground-state Nile Red.

MATERIALS AND METHODS

Chemicals. Nile Red (NR), 7-diethylamino-3,4-benzophenoxazine-2-ona, was purchased from Bio Chemika (Sigma for Fluorescence), and poly(*n*-alkyl) methacrylates (PAMA), *n*-butyl (PBMA, M_w = 337.000), ethyl (PEMA, M_w = 350.000), and methyl (PMMA, M_w = 350.000) were from Sigma-Aldrich, and were used as received. Molecular structures are given in Scheme 1. Toluene was from Sigma-Aldrich (spectroscopic grade).

Scheme 1. Molecular Structure of Dye and Polymers

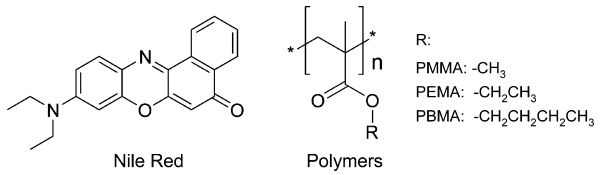

Polymer Film Preparation and Characterization. Polymer solutions were prepared in toluene at different concentration to control the deposited film thickness by spin coating. (See later.) They contained NR at the adequate proportion to the polymer. For ensemble measurements, we employed a dye concentration of 10^{-7} mol/kg of polymer, guaranteeing that no aggregates were formed and minimizing FRET effects among dye molecules. For SM measurements, a concentration of 10^{-12} mol/kg of polymer was used. Coverslip substrates (Menzel-Gläser, no. 1.5) and all glass material employed for sample preparation were rigorously cleaned, rinsed with solvents (acetone, methanol, and Milli-Q water) and exposed to UV and O_3 for 30 min in an ozonizer (UVO Cleaner, model 42A-220, Jelight Company). Polymer concentrations ranging from 0.25 to 2.00% w/w in toluene were used. Thin polymer films were obtained by spin coating the polymer−dye solutions onto the substrate. The films were dried in vacuum at 323 K for 12 h. Film thickness of 200 and 25 nm was measured by profilometry (Veeco, Dektak 3ST).[35] Roughness, characterized by AFM, was <2% (constant force = 0.852 N and scan speed 1.02 Hz, processed by Nanoscope II).

Ensemble and Single-Molecule Fluorescence Anisotropy. Both types of measurements were carried out at room temperature in an Olympus IX71 inverted microscope. A laser diode (SDL-532-200T, Shanghai Dream Lasers Technology) at 532 nm was used to excite the sample. The laser output power was tuned by a wedge-shaped neutral filter. A shutter allowed excitation light interruption when necessary. A polarizer and a retarding plate were used to achieve a linearly polarized excitation over the sample. (The excitation power ratio between the two orthogonal directions after the objective was 1/200.) Typical laser power at the sample location was in the range: 0.18 to 0.70 mW (corresponding to $(2-8) \times 10^{20}$ photons·cm^{-2}·s^{-1} on the analyzed area of the ensemble photobleaching experiments: 60 μm^2). Dichroic mirror and emission filter were chosen for Nile Red spectroscopic features (Semrock TRITC cube). An oil-immersion objective (Olympus, PLAN APO N 60×, NA 1.42) focused for wide-field irradiation was used. In the emission channel, a filter wheel with two polarizers in adjacent positions aligned parallel and perpendicular to excitation polarization direction allowed us to capture sequentially both emission components. The fluorescence signal was detected by an Andor iXon-885 EMCCD camera. Exposure time was 0.1 s for each polarization direction. The

time between successive exposures was limited by the rotation of the filter wheel to 1.1 s. In the systems studied, the time in which dye reorientation changes take place lies in the tens of seconds range,[18] and thus the acquisition time is short enough. In SM experiments, we used stroboscopic excitation to decrease photobleaching: an irradiation period of 1.1 s, adequate to record a parallel, and a perpendicular frame, was followed by 10 s of darkness. This allowed measurements of several minutes (and up to 1 h) before considerable photobleaching was observed within the studied area. In ensemble experiments, we used continuous excitation.

To take into account the different sensitivity of detection to light polarization orientation, usually denoted as G factor (see eq 1), we calibrated the microscope detection channel using a concentrated ensemble film whose steady-state anisotropy was measured in a PTI-Quantamaster spectrofluorometer equipped with polarizers. All NR samples used had steady-state anisotropy of 0.39 ± 0.01. The correct G factor could reproduce in the microscope (just before photobleaching begins to have a significant effect) the same steady-state anisotropy as measured in the fluorometer.

Anisotropy was calculated using successive images taken parallel and perpendicular to the polarization of the excitation.[36] For ensemble measurements, the intensity was averaged in the entire viewing field, where $I > 0.9I_{max}$. (The space distribution of the incident irradiation beam was Gaussian with a very good degree of approximation.) For SM measurements, the intensity was added in all pixels of a diffraction limited spot, corresponding to the image of one molecule. In all cases, the anisotropy at each time, $r(t)$, after correction for background signal, was calculated as[37]

$$r(t) = \frac{I_{//} - B - G(I_{\perp} - B)}{I_{//} - B + 2G(I_{\perp} - B)} \quad (1)$$

where $I_{//}$ and $I_{\perp}$ are the intensities parallel and perpendicular to the excitation polarization direction, respectively, and the background noise, B, was determined as the mean of the signal acquired by the camera when no dye was employed in the preparation of the sample while all other irradiation and detection conditions were kept constant. SM emission anisotropy time traces were obtained for ca. 250 molecules in each film.

To identify molecules in an image sequence, we employed a Matlab routine[38] that selects the brightest spots after adding all frames. To minimize the influence of noise (due to electronics or to scattered light) and to correct for inhomogeneities in the excitation intensity, we subtracted from every frame the result of a Gaussian filter.[39] Identifying molecules after adding all frames allows for also locating those that were in a dark state at the beginning of the sequence.

RESULTS

1. Single Molecule. Single-molecule polarized intensity time traces are shown in Figure 1. Figure 1A shows a molecule time trace in PMMA, and Figure 1B shows a molecule time trace in PBMA. Molecules are monitored until one-step photobleaching takes place. The upper panel of each molecular trace shows the parallel (blue) and perpendicular (red) intensity as well as the operative total intensity (black), calculated as $I_{tot} = I_{\|} + 2GI_{\perp}$. The lower panel shows the time evolution of the anisotropy. SM anisotropy values span the entire possible range, that is, $-0.5 \leq r \leq 1.0$.

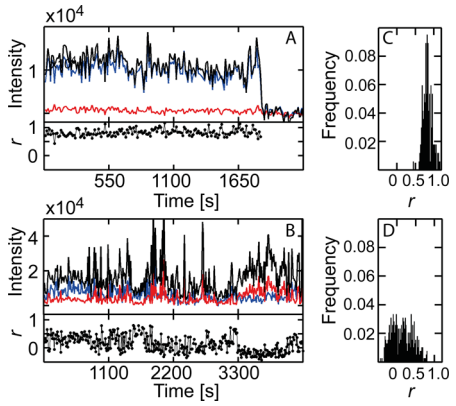

Figure 1. Single-molecule polarized emission intensity and anisotropy time traces of NR in 200 nm films of PMMA (A) and PBMA (B). A and B upper panels show $I_{\|}$ (blue line), $GI_{\perp}$ (red line), and operative total intensity ($I_{\|} + 2GI_{\perp}$; black line) is expressed in counts/100 ms. The bottom panels show the corresponding anisotropy. For the molecule in panel A, the anisotropy calculation is performed until photobleaching occurs. Panels C and D show the frequency histogram for the anisotropy of molecules in panels A and B, respectively.

Different behaviors are observed. In PMMA, anisotropy fluctuations are quite low. For example, in Figure 1A, the time trace of a SM in PMMA can be described, over the observed time interval, by an approximately time-independent average value of the anisotropy of $\langle r \rangle = 0.83$ with a small mean-square deviation of 0.11. The example illustrated in PBMA in Figure 1B has a larger variation over time, which is typical of the behavior in PBMA, as compared with PMMA at room temperature. The molecule in this trace can be characterized by $\langle r \rangle = 0.14$, over the entire observation time, with a mean-square deviation of 0.28, but its behavior more greatly resembles a diffusion-type trajectory. Still molecule in Figure 1B depicts another frequent behavior: a change between different dynamic ranges. Around 1600 s, there is a sudden slowing down of the fluctuation for 100 s, after which the dynamics recovers its previous behavior. Also, at 3300 s, the orientation and the mobility of the molecule changes suddenly in the observation time domain: from a situation that can be described by $\langle r \rangle = 0.23$ and mean-square displacement of 0.26 (at $t < 3300$ s) to an orientation characterized by $\langle r \rangle = -0.19$ and a mean-square displacement of 0.12 (at $t > 3300$ s). This means that at 3300 s the cage experienced a major rearrangement. This change is much rarer than the frequent reorientations around an essentially constant average value. This type of behavior is more often found in PBMA than in PMMA at room temperature.

Figure 2 shows two quite different behaviors in PBMA. On one side is molecule A with large anisotropy fluctuations ($\langle r(t) \rangle = 0.10 \pm 0.33$). On the other side is molecule B, with small anisotropy fluctuations around a mean value ($\langle r(t) \rangle = -0.29 \pm 0.09$). This demonstrates the existence of very rigid environ-

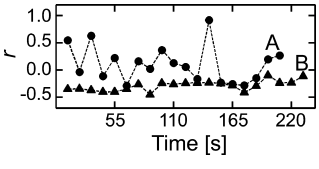

Figure 2. Emission anisotropy time traces for two Nile Red molecules (A and B) in a 200 nm PBMA film.

dx.doi.org/10.1021/jp500272y | J. Phys. Chem. A 2014, 118, 10309−10317

ments and others with a very high mobility as a result of spatial heterogeneity.

The two last examples described are typical of what in polymer environments is commonly referred to as time heterogeneity (change in the dynamics of a single cage, molecule in Figure 1B) and spatial heterogeneity (different dynamics in different locations, Figure 2).

A common way to investigate fluctuations in SM experiments is to use autocorrelation functions.[38,40] However, this method requires measurements containing several thousands of succeeding data points taken during the time of investigation. In our experiments, acquisition of sufficient data points was prevented by photobleaching. For this reason, we calculate the square of the difference in anisotropy of successive determinations along the time traces and compute the complementary cumulative distribution function (CCDF), $\Phi_c(\Delta r^2)$, as defined in eq 2 for the probability distribution function $g(\Delta r^2)$. It expresses the probability of observing an anisotropy change larger than a certain absolute value,[41,42] Δr_k

$$\Phi_c(\Delta r_k^2) = \int_{\Delta r_k^2}^{\infty} g(\Delta r^2)\, d\Delta r^2 \tag{2}$$

To statistically analyze the results, we gather all anisotropy variations of all SMs detected in each polymer and for each film thickness and build the corresponding $\Phi_c(\Delta r^2)$. Figure 3 shows

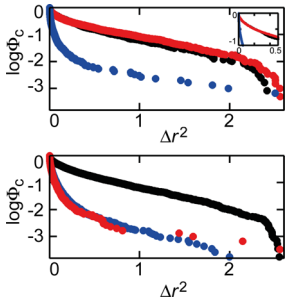

Figure 3. Logarithm of the complementary cumulative distribution for the square of anisotropy changes (log $\Phi_c(\Delta r^2)$) for all NR molecules measured at room temperature in PMMA (blue circles), PEMA (red circles), and PBMA (black circles) films of 25 nm (top panel) and 200 nm thickness (bottom panel). The inset in the top panel shows a detail of the lower anisotropy fluctuation range.

the results for PBMA, PEMA, and PMMA thin films of 25 and 200 nm. The orientation fluctuations of NR present very different behavior in PBMA compared with PMMA. This is related to the polymer rigidity and is independent of film thickness in these polymers. While in PMMA 85% of anisotropy fluctuations of NR take place with $|\Delta r| < 0.20$, this proportion is only 38% in PBMA.

As opposed to the other two polymers, in PEMA, a distinct behavior is observed for $\Phi_c(\Delta r^2)$ of NR with the change in film thickness. Large fluctuations ($|\Delta r| > 0.20$) are more frequent in 25 nm than in 200 nm films. Moreover, the general trend in PEMA films of 25 nm resembles the behavior in PBMA films, whereas the distribution of fluctuations in the 200 nm film matches the distribution found in PMMA films at the same temperature (Figure 3, top and low panels, respectively). The changes of the in-cage mobility of NR in the polymer films are in line with the thickness dependence of the glass-transition processes.[14,43] The more frequent observation of large fluctuations in orientation is expected in flexible environments, and this flexibility increases very fast some degrees under and above T_g. The change in T_g with film thickness is still a matter of debate, and frequently different techniques applied to the same polymer render controversial results because the T_g displacement depends on polymer nature, underlying substrate, film processing, and molecular weight.[44] The bulk T_g of PMMA is 388 K. This value is too high compared with room temperature to show any mobility difference, even considering that for this polymer, films of <25 nm thickness have a T_g 8 K above the bulk. In the case of PEMA, the T_g of the bulk is 334 K, while the T_g of 25 nm films is 320 K.[14] This temperature, ~24 K higher than the temperature of the measurements, is low enough to display the increase in mobility typical for the neighborhood of T_g. In this way, in PEMA, the orientation mobility of NR increases as the film thickness decreases, in agreement with the decrease in T_g due to nanoconfinement effects. We found no data available in the literature for thin films of PBMA, but its T_g bulk = 298 K explains the observed high orientation mobility of NR in all cases.

2. Ensemble Measurements. Figure 4 shows the results of the time variation of the anisotropy of NR in thin films of

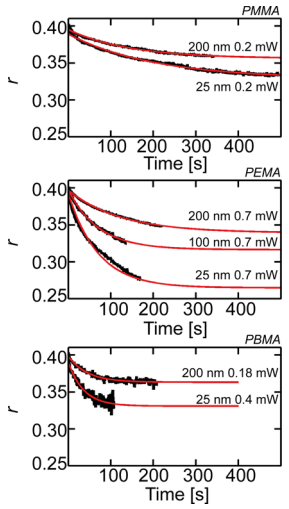

Figure 4. Experimental anisotropy decay of NR in PMMA, PEMA, and PBMA (black traces from top to bottom) as a function of time during continuous irradiation at 532 nm with linearly polarized light of polymer films with thickness of 200, 100, and 25 nm. The best fits to the results given by eq 7 are shown as continuous red curves.

PMMA, PEMA, and PBMA under linearly polarized irradiation causing photobleaching. The anisotropy decays monotonously in all cases as a result of irradiation with linearly polarized light. This is a consequence of selective photobleaching of molecules oriented in a small angle relative to the direction of the incident polarized light. For long times, the anisotropy reaches a constant value (r_∞) in all cases. This is a result of the existence of two processes that alter the angular distribution of molecules in the ground state and that operate in opposite directions and at the same rate at this point: orientational-dependent depopulation by polarized photobleaching and recovery by rotational diffusion. The experiment shows a way to take advantage of the unavoidable photobleaching to study the effect of rotational diffusion. This experiment bears similarities to fluorescence recovery after photobleaching or hole burning.

dx.doi.org/10.1021/jp500272y | J. Phys. Chem. A 2014, 118, 10309−10317

DISCUSSION

For SMs, the analysis based on $\Phi_c(\Delta r^2)$ shows different mobility for different environments. The results demonstrate that SM anisotropy measurements allow for sensing changes of in-cage mobility previous to the cooperative movements that give rise to glass transition.[45,46] The increasing SM anisotropy fluctuations are the molecular level manifestation of the increase in mobility that leads to the glass−rubber transition. Our results show that orientation fluctuation of SM is a good spectroscopical indication at the microscopic level of the cooperative macroscopic changes. In a previous work, we observed that spectral fluctuations were not able to sense this difference in the same polymer environments.[35] We explain this fact by assuming that spectral fluctuations depend on small movements of the dye in the polymer cage that slightly change the distance between critically interacting probe and polymer functional groups. On the contrary, reorientation of NR requires a concerted movement of the cage to accommodate the dye in a different position. This rearrangement is more sensitive to the mobility of the polymer backbone responsible for the changes around T_g, as depicted in Scheme 2.

Scheme 2. Schematic Representation of NR Movements in the Polymer Cage, Responsible for the Spectral Changes (Blue Vertical Arrow) and for the Rotational Reorientation (Curved Red Arrow)[a]

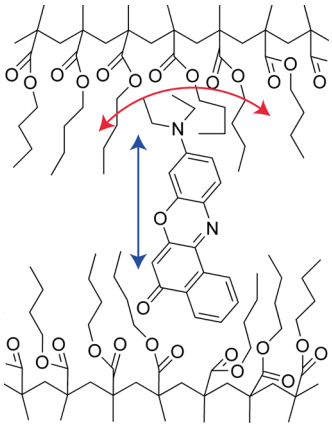

[a]PBMA is taken as representative structure.

This result clearly shows the change in dynamical regime. Contrary to the calculation of correlations from individual fluorescence time traces, the probability distributions do not contain information on individual time behavior, from which rotational diffusion coefficients could be calculated. As previously explained, we could not obtain reasonably long time trajectories suitable for a time correlation analysis. However, as long as the molecular dipoles do show only small angular changes within the employed time steps of 11 s between succeeding determinations of the orientation, the angular variations can be used to determine rotational diffusion coefficients.[11] The in-plane angular position α is derived as $\alpha = \arctan(I_\perp/I_{//})^{1/2}$, for all molecules in the same type of polymer film to obtain the angular displacement $\Delta\alpha$ for the time interval between successive measurements $\Delta t = 11$ s. The variations of this angle α are related to the rotational diffusion coefficient D by

$$<\Delta\alpha^2> = D/(2\cdot\Delta t) \tag{3}$$

The values of D calculated in this way are given in Table 1. They follow the trend pointed out by $\Phi_c(\Delta r^2)$ and compare well with the respective values obtained from the ensemble measurements. (See later.)

The ensemble experiments need a model that can quantitatively account for the time-dependent behavior of the steady-state anisotropy to obtain values for the photobleaching rate and for the rotational diffusion coefficient. To achieve this, we must make some assumptions that are explained in what follows.

Photobleaching is assumed to be an irreversible single photon process that carries the dye irreversibly to a dark state. Because the dye molecules are embedded in a rigid matrix, the lifetime of the excited state is much shorter than the mean time, at which a change in orientation occurs and therefore no rotational diffusion takes place in the excited state, and a molecule emits the fluorescence photon in the same orientation as the absorption took place. Therefore, we are monitoring changes in the orientation of the ground state. Moreover, because NR in all of these polymer films has a steady-state anisotropy value very close to the limiting anisotropy of 0.4 in a randomly oriented sample, this confirms the absence of significant depolarization in the excited state and shows the fact that absorption and emission dipoles are almost parallel.

Under linearly polarized excitation, the absorption rate, $I_a(\theta,t)$ is

$$I_a(\theta, t) = I_0\cdot\sigma\cdot N(\theta, t)\cdot\cos^2\theta \tag{4}$$

where σ is the absorption cross section for polarized excitation, I_0 is the incident photon density per unit area and time, θ is the angle between polarization direction and the molecular absorption dipole moment, and $N(\theta,t)$ is the instantaneous angular distribution of molecules in the ground state.

Table 1. Parameters (τ_{op} and r_∞) Obtained by Fitting the Experimental Ensemble Steady-State Anisotropy Decays with Equation 7 and Corresponding Values of D and Φ Computed by Using These Parameters with Equations 8 and 9[a]

polymer	thickness [nm]	τ_{op} [s] ±15%	r_∞ ± 0.005	D [× 10^{-3} s^{-1}] ± 30%	Φ [10^{-3} s^{-1}] ± 30%	ϕ_b [× 10^{-9}] ± 30%	D_{SM} [× 10^{-3} s^{-1}] ± 20%
PMMA	200	144	0.360	1.2	1.3	3	1.0
	25	202	0.332	0.8	1.4	3	0.8
PEMA	200	124	0.340	1.4	2.1	6	0.9
	100	70	0.321	2.7	5.4	15	nd
	25	69	0.260	2.2	7.3	20	6.9
PBMA	200	44	0.361	4.3	4.0	45	7.1
	25	36	0.330	5.4	9.1	43	6.7

[a]The quantum yield ϕ_b is derived as $\phi_b = \Phi/I_0\sigma$ ($\sigma_{RN} = 4.2 \times 10^{-16}$ cm^2 and I_0 was between (2 and 8) × 10^{20} photons·cm^{-2}·s^{-1}; analyzed area: 60 μm^2). Values of the rotational diffusion coefficient calculated from the single-molecule experiments are given in column D_{SM}.

dx.doi.org/10.1021/jp500272y | J. Phys. Chem. A 2014, 118, 10309−10317

Considering a photobleaching that takes place after single photon absorption with a quantum yield ϕ_b and the known equation for rotational diffusion,[34] the rate expression for $N(\theta,t)$ can be written as

$$\frac{\partial N(\theta,t)}{\partial t} = -\phi_b \cdot I_0 \cdot \sigma \cdot \cos^2\theta \cdot N(\theta,t) + D\left[\frac{1}{\sin\theta}\cdot\frac{\partial}{\partial\theta}\left(\sin\theta\cdot\frac{\partial N(\theta,t)}{\partial\theta}\right)\right] = -\Phi\cos^2\theta\cdot N(\theta,t) + D\left[\frac{1}{\sin\theta}\cdot\frac{\partial}{\partial\theta}\left(\sin\theta\cdot\frac{\partial N(\theta,t)}{\partial\theta}\right)\right] \quad (5)$$

where $\Phi = I_0\sigma\phi_b$. Note the fact that no dependence in the other orientation angle ϕ exists because of the cylindrical symmetry of the excitation−emission geometry. Given the nature of the dye used in this work,[47] we can assume isotropic rotational diffusion (i.e., a scalar diffusion coefficient). To solve this equation, we consider a solution in the form of a series

$$N(\theta,t) = \sum_{l=0}^{\infty} C_l(t)\cdot P_l(\cos\theta) \quad (6)$$

where P_l are the Legendre polynomials of l order and C_l are time-dependent coefficients. By using the recurrence relations for the Legendre polynomials, we arrive to a system of linear differential equations for the coefficients C_l. (See the SI for further development.)

The solution to the system is straightforward with numerical software. The series expansion of eq 6 must be truncated considering a proper amount of coefficients for an adequate description of the experimental results, fixing the dimension of the system of equations for the coefficients C_l. We found out that using 16 terms in the series expansion was sufficient to describe the results with adequate accuracy. The initial condition was a homogeneous distribution, giving an initial value of 0.4 for the anisotropy. Determination of the set of C_l (eq 6) will allow us to determine $N(\theta,t)$ and from it the time-dependent steady-state anisotropy. (See the SI.)

The fit of experimental data to the solution of eq 5 with two adjustable parameters, D and Φ, and an initial condition r (t = 0) = 0.4 is not straightforward. In what follows, we propose a simplified method overcoming the fit to the integral equation; instead, the data are fitted to an equivalent and simpler, operative expression. For this, we built a large set of curves by systematically varying D and Φ in adequate intervals. In Figure 5, some of these curves are shown. They have three common features: (1) $r(t)$ decays until both processes, photobleaching and reorientations, are balanced, rendering a constant r_∞; (2) sets of curves with constant ratio D/Φ have the same r_∞ value, and the lower the value of D/Φ, the lower r_∞; and (3) the smaller the value of D, $r(t)$ decays more slowly.

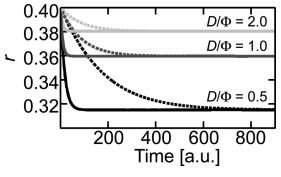

Figure 5. Calculated steady-state anisotropy decays from numerical integration of eq 5 for different values of D/Φ. Dotted lines have values of D and Φ 10 times smaller than the corresponding full line while keeping D/Φ constant. Parameters: D/Φ = 2.0: solid line, D = 0.02, Φ = 0.01; dotted line, D = 0.002; Φ = 0.001. D/Φ = 1.0: solid line, D = 0.02, Φ = 0.02; dotted line, D = 0.002, Φ = 0.002. D/Φ = 0.5: solid line, D = 0.01, Φ = 0.02; dotted line, D = 0.001, Φ = 0.002.

The results in Figure 5 suggest a simple anisotropy time dependence with the following functional dependence:

$$r(t) = (0.4 - r_\infty)\cdot\exp(-t/\tau_{op}) + r_\infty \quad (7)$$

The fitting parameters r_∞ and τ_{op}, are operative values that must be related to the parameters of the model: D and Φ. To obtain the relation between these sets of parameters, we performed the fit to eq 7 of the decays obtained by solving eq 5 (Figure 5). This procedure renders the correlations of Figure 6 that can be represented by the following relationships:

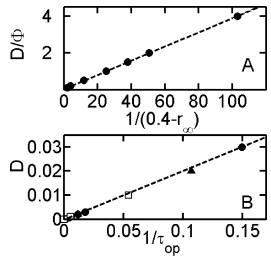

Figure 6. Correlation between the parameters of eqs 5 and 7. In the lower panel: open squares, D/Φ = 0.5; full circles, D/Φ = 1.0; and full triangles, D/Φ = 2.0.

$$\frac{D}{\Phi} = \frac{(0.038 \pm 0.001)}{0.4 - r_\infty} + (0.040 \pm 0.001) \quad (8)$$

$$D = (0.20 \pm 0.04)\frac{1}{\tau_{op}} - (2\times10^{-4} \pm 1\times10^{-4})\ \mathrm{s}^{-1} \quad (9)$$

Equations 8 and 9 can be used to obtain D and Φ by fitting the steady-state anisotropy decays to eq 7 (the red full lines of Figure 4 were obtained in this way), a much simpler procedure than performing the integration of eq 5. The results of this procedure are presented in Table 1. The proposed model of single-photon photobleaching and isotropic dye rotations is in good agreement with the experimental anisotropy decays.

ϕ_b values reported in literature for fluorophores used frequently in SM experiments (for Rhodamines: R6G, R123, and TMR) are in the range 10^{-4} to 10^{-9},[48] and our results for NR are between 10^{-7} and 10^{-9}, indicating the good stability of this dye in poly(alkyl methacrylates). In PBMA, NR shows the highest photobleaching quantum yield, while in PMMA it displays the lowest, independent of film thickness. This tendency parallels the trend in D and in O_2 permeability in the polymers. ϕ_b can be expressed as

$$\phi_b = \frac{k_R[O_2]}{k_R[O_2] + 1/\tau_0} \approx \tau_0 k_R[O_2] \quad (10)$$

where k_R is the reactive rate constant of the dye with oxygen and τ_0 is the dye's excited-state lifetime. The diffusion-limited encounters of dye and oxygen establish the upper limit for the reactive rate constant

$$k_R = 4\pi\cdot N_A\cdot d\cdot D_{O2} \quad (11)$$

dx.doi.org/10.1021/jp500272y | J. Phys. Chem. A 2014, 118, 10309−10317

in which d is the distance between the centers of the species forming the encounter complex and D_{O2} is the diffusion coefficient of molecular oxygen.

The permeability, P, is defined as the product of the sorption coefficient, S, and the diffusion coefficient: $P = SD$. If we assume that $[O_2]$ in the polymer is proportional to the oxygen partial pressure, then pO_2,$[O_2] = S{\cdot}pO_2$ and

$$k_R[O_2] = 4\pi{\cdot}N_A{\cdot}d{\cdot}D_{O2}{\cdot}[O_2] = 4\pi{\cdot}N_A{\cdot}d{\cdot}P{\cdot}pO_2 \quad (12)$$

This proportionality between k_R and P of oxygen in the polymer was experimentally previously found.[49] So the photobleaching quantum yield is also proportional to P. This parameter decreases with polarity increase for molecular oxygen but also with the difference between T and T_g at $T < T_g$.[50] Furthermore, the magnitude of $P = 5.2 \times 10^{-20}$ mol/(cm s Pa) (for PMMA at room temperature) predicts a values of ϕ_b of the order of 8×10^{-7} under atmospheric conditions (pO_2 = 21 kPa) for an excited-state lifetime of 1 ns and d = 1 nm. For PEMA, P for oxygen is 4.0×10^{-19} mol/(cm s Pa), leading to ϕ_b on the order of 6×10^{-6} under the same conditions. So oxygen permeability can explain the trend in ϕ_b as well as its broad variability, and these facts point to the presence of O_2 in the matrix as the principal agent in the photobleaching reaction.

The rotational diffusion coefficient obtained from ensemble measurements agrees in its tendency from what can be deduced from the SM experiments of Figure 3. Moreover, the quantitative agreement between the two types of experiments is quite good. For the three most rigid films: PMMA of 25 and 200 nm and for PEMA of 200 nm, the agreement is excellent. In this case, the angular fluctuations are small enough to support calculations using the projection angle instead of the 3D fluctuation.[11] For the most flexible films, the agreement is not so good. In PBMA, the values of D derived from SM experiments are ca. 50% higher than the ones obtained from the ensemble measurements. In PEMA of 25 nm thickness, the value of D obtained from SM experiments is similar to the value in PBMA, as the curves in Figure 3 show, but it is a factor of three higher than the value derived from the ensemble measurements. Nevertheless, the tendency to less rigid environments as the polymer film thickness decreases in PEMA is shown in both types of measurements. The rotational diffusion coefficient derived for the 100 nm film in PEMA fits very well into this picture. The magnitude of the rotational diffusion coefficients measured for NR in poly(alkymethacrylates) is of the expected order, literature reports give $D = 10^{-4}$ s^{-1} for 4-dimethylamino-4′-nitrostilbene in PMMA at 10 K below T_g,[19] $D = 8.3 \times 10^{-3}$ s^{-1} for a perylene diimide in poly(methyl acrylate) at 294 K,[11] $D = 1.9 \times 10^{-3}$ s^{-1} for Rhodamine B in poly(vinylacetate) at the T_g (305 K),[20] and $D = 73 \times 10^{-3}$ s^{-1} for a BODIPY dye in poly(methyl acrylate) at 285 K (3 K above T_g for the sample).[21]

A drawback in the ensemble model we developed concerns its neglect of the heterogeneous nature of polymer samples, which is evident in the SM measurements. The data, nevertheless, show this heterogeneous nature. This is represented in Figure 7, where the ensemble steady-state anisotropy decay is represented and fitted to eq 7 in the same experiment but restricting the analysis to different time intervals covering the photobleaching of 70 and 90% of the total initial emission intensity. When different proportions of molecules are photobleached in the same sample, the calculated D and Φ values vary. In the example discussed, D and Φ are 21×10^{-3} s^{-1} and 10×10^{-8}, 6.5×10^{-3} s^{-1} and 5.3×10^{-8}, and 4.3×10^{-3} s^{-1} and 4.5×10^{-8}, for 70, 80 (data not shown), and 90% photobleaching, respectively. D decreases when the photobleached population proportion increases. This fact can be explained by the differences in the polymer cage flexibility brought to light by SM experiments. At the beginning of the experiments, molecules with fast and slow dynamics set the ensemble D value. Under continuous irradiation, molecules with fast rotational dynamics and the slow ones that lie preferentially oriented with the direction of the linearly polarized electromagnetic field are more likely to be photobleached than the others. This selective bleaching based on rotational motion is the origin of the observed decrease in the ensemble average value of D, as the experiment progresses. This conclusion was also found in rotational correlation time studies of rubrene in polystyrene films.[51] The change in photobleaching quantum yield follows the same tendency, and this can also be explained by the lower mobility of oxygen in the remaining more rigid sites.

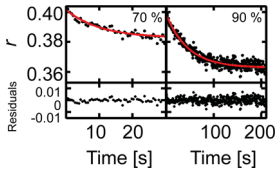

Figure 7. Upper plots: Anisotropy decay of NR in PBMA of 200 nm film thickness after 70 and 90% photobleaching of the initial emission signal (dotted black points) and its corresponding fittings to eq 7 (continuous red line). Bottom plots: fitting residuals. Laser power: 0.18 mW at 532 nm.

CONCLUSIONS

We have conducted two different types of experiments with NR-doped poly(alkyl methacrylate) films of nanometric thickness: SM and ensemble measurements. The two approaches converge to confirm a complete picture of the time and spatial heterogeneous dynamics typical of the polymer glassy state: as in previous works, the present results confirm that spatial heterogeneity is more important than time heterogeneity. This is the most important contribution of the SM experiments, which also give a quantitative hint of the value of the rotational diffusion coefficient. For rigid polymers, SM experiments yield even qualitative rotational diffusion coefficients. Ensemble experiments provide a more trustful value of this parameter but lack the direct observation of heterogeneity, which is only insinuated through the analysis of different time intervals. The remarkable point of this work is the quantitative coincidence of ensemble and SM experiments. This confirms that SM experiments are dealing with representative ensembles and that ensemble experiments can give apparent homogeneous behaviors despite the underlying spatial and time heterogeneity of the sample.

Additionally, we develop a simple model to describe the dynamics of the ensemble, which is simple to use, takes advantage of the unavoidable photobleaching and shows a good agreement with experiments, also allowing for retrieving both rotation and bleaching parameters.

ASSOCIATED CONTENT

Supporting Information

Solution of the differential equation for diffusion and polarized photobleaching and consideration of nonparallel absorption and emission transition moments for this mathematical

dx.doi.org/10.1021/jp500272y | J. Phys. Chem. A 2014, 118, 10309−10317

treatment. This material is available free of charge via the Internet at http://pubs.acs.org.

AUTHOR INFORMATION

Corresponding Authors

*C.v.B.: borczyskowski@physik.tu-chemnitz.de; Tel: +4937153133035

*P.F.A.: pedro.aramendia@cibion.conicet.gov.ar ; Tel: +541148995590.

Present Address

⊥A.C.: Leiden Institute of Physics, Leiden University, Niels Bohrweg 2, 2333 CA Leiden, Netherlands.

Notes

The authors declare no competing financial interest.

ACKNOWLEDGMENTS

P.F.A. is a staff member of Carrera del Investigador Científico from Consejo Nacional de Investigaciones Científicas y Técnicas (CONICET, Argentina). B.A. performed her work with doctoral fellowships from ANPCyT (Grant PICT 34193) and CONICET. The work was performed under financial support from UBA (grant 20020100100234), CONICET (grant 11220100100397), DAAD-MINCyT grant 0807, and DFG-FOR 877. We thank Mario Heidernätsch and Stefan Krause (both TUC, Germany) for helpful discussions.

REFERENCES

(1) Yu, Y.; Ikeda, T. Alignment Modulation of Azobenzene-Containing Liquid Crystal Systems by Photochemical Reactions. *J. Photochem. Photobiol., C* **2004**, *5*, 247−265.

(2) Finkelmann, H.; Nishikawa, E.; Pereira, G. G.; Warner, M. A New Opto-Mechanical Effect in Solid. *Phys. Rev. Lett.* **2001**, *87*, 15501−15504.

(3) Richert, R. Evidence for Dynamic Heterogeneity near T_g from the Time-Resolved Inhomogeneous Broadening of Optical Line Shapes. *J. Phys. Chem. B* **1997**, *101*, 6323−6326.

(4) Richert, R.; Heuer, A. Rate-Memory and Dynamic Heterogeneity of First-Order Reactions in a Polymer Matrix. *Macromolecules* **1997**, *30*, 4038−4041.

(5) Wei, C.-Y. J.; Kim, Y. H.; Darst, R. K.; Rossky, P. J.; Vanden Bout, D. A. The Origins of Non-Exponential Decay in Single Molecule Measurements of Rotational Dynamics. *Phys. Rev. Lett.* **2005**, *95*, 173001−173005.

(6) Myers, A. B.; Tchenio, P.; Moerner, W. E. In *Advanced Optical Methods for Ultrasensitive Detection*; Fearey, B. L., Ed.; SPIE: Bellingham, WA, 1995; Vol. *2385*, pp 103−114.

(7) Barkai, E.; Jung, Y.; Silbey, R. Theory of Single-Molecule Spectroscopy: Beyond the Ensemble Average. *Annu. Rev. Phys. Chem.* **2004**, *55*, 457−507.

(8) Ambrose, W. P.; Moerner, W. E. Fluorescence Spectroscopy and Spectral Diffusion of Single Impurity Molecules in a Crystal. *Nature* **1991**, *349*, 225−227.

(9) Vallée, R. A. L.; Cotlet, M.; Van Der Auweraer, M.; Hofkens, J.; Müllen, K.; De Schryver, F. C. Single Molecule Conformations Probe-Free Volume in Polymers. *J. Am. Chem. Soc.* **2004**, *126*, 2296−2297.

(10) Schob, A.; Cichos, F.; Schuster, J.; von Borczyskowski, C. Reorientation and Translation of Individual Dye Molecules in a Polymer Matrix. *Eur. Polym. J.* **2004**, *40*, 1019−1026.

(11) Adhikari, S.; Selmke, M.; Cichos, F. Temperature Dependent Single Molecule Rotational Dynamics in PMA. *Phys. Chem. Chem. Phys.* **2011**, *13*, 1849−1856.

(12) Wöll, D.; Braeken, E.; Deres, A.; De Schryver, F. C.; Uji-i, H.; Hofkens, J. Polymers and Single Molecule Fluorescence Spectroscopy, What Can We Learn? *Chem. Soc. Rev.* **2009**, *38*, 313−328.

(13) Flier, B. M. I.; Baier, M. C.; Huber, J.; Müllen, K.; Mecking, S.; Zumbusch, A.; Wöll, D. Heterogeneous Diffusion in Thin Polymer-Films as Observed by High-Temperature Single Molecule Fluorescence Microscopy. *J. Am. Chem. Soc.* **2012**, *134*, 480−488.

(14) Priestley, R. D.; Mundra, M. K.; Barnett, N. J.; Broadbelt, L. J.; Torkelson, J. M. Effects of Nanoscale Confinement and Interfaces on the Glass Transition Temperatures of a Series of Poly(n-methacrylate) Films. *Aust. J. Chem.* **2007**, *60*, 765−771.

(15) Keddie, J. L.; Jones, R. A. L.; Cory, R. A. Size-Dependent Depression of the Glass Transition Temperature in Polymer Films. *Europhys. Lett.* **1994**, *27*, 59−64.

(16) Jackson, C. L.; McKenna, G. B. The Glass Transition of Organic Liquids Confined to Small Pores. *J. Non-Cryst. Solids* **1991**, *131*−*133*, 221−224.

(17) Ha, T.; Glass, J.; Enderle, T.; Chemla, D. S.; Weiss, S. Hindered Rotational Diffusion and Rotational Jumps of Single Molecules. *Phys. Rev. Lett.* **1998**, *80*, 2093−2096.

(18) Zondervan, R.; Kulzer, F.; Berkhout, G. C. G.; Orrit, M. Local Viscosity of Supercooled Glycerol Near T_g Probed by Rotational Diffusion of Ensembles and Single Dye Molecules. *Proc. Natl. Acad. Sci. U.S.A.* **2007**, *104*, 12628−12633.

(19) Liu, L.-Y.; Ramkrishna, D.; Lackritz, H. S. Rotational Brownian Motion of Chromophores and Electric Field Effects in Polymer Films for Second Order Nonlinear Optics. *Macromolecules* **1994**, *27*, 5987−5999.

(20) Bingemann, D.; Allen, R. M.; Olesen, S. W. Single Molecules Reveal the Dynamics of Heterogeneities in a Polymer at the Glass Transition. *J. Chem. Phys.* **2011**, *134*, 024513.

(21) Hinze, G.; Basché, T.; Vallée, R. A. L. Single Molecule Probing of Dynamics in Supercooled Polymers. *Phys. Chem. Chem. Phys.* **2011**, *13*, 1813−1818.

(22) Harms, G. S.; Sonnleitner, M.; Schütz, G. J.; Gruber, H. J.; Schmidt, T. Single-Molecule Anisotropy Imaging. *Biophys. J.* **1999**, *77*, 2864−2870.

(23) Paeng, K.; Swallen, S. F.; Ediger, M. D. Direct Measurement of Molecular Motion in Freestanding Polystyrene Thin Films. *J. Am. Chem. Soc.* **2011**, *133*, 8444−8447.

(24) Habuchi, S.; Oba, T.; Vacha, M. Multi-Beam Single-Molecule Defocused Fluorescence Imaging Reveals Local Anisotropic Nature of Polymer Thin Films. *Phys. Chem. Chem. Phys.* **2011**, *13*, 7001−7007.

(25) Börner, R.; Kowerko, D.; Krause, S.; von Borczyskowski, C.; Hübner, C. G. Efficient Simultaneous Fluorescence Orientation, Spectrum, and Lifetime Detection for Single Molecule Dynamics. *J. Chem. Phys.* **2012**, *137*, 164202−11.

(26) Jung, C.; Hellriegel, C.; Platschek, B.; Wöhrle, D.; Bein, T.; Michaelis, J.; Bräuchle, C. Simultaneous Measurement of Orientational and Spectral Dynamics of Single Molecules in Nanostructured Host-Guest Materials. *J. Am. Chem. Soc.* **2007**, *129*, 5570−5579.

(27) Ruiter, A. G. T.; Veerman, J. A.; Garcia-Parajo, M. F.; van Hulst, N. F. Single Molecule Rotational and Translational Diffusion Observed by Near-Field Scanning Optical Microscopy. *J. Phys. Chem. A* **1997**, *101*, 7318−7323.

(28) Weston, K. D.; Goldner, L. S. Orientation Imaging and Reorientation Dynamics of Single Dye Molecules. *J. Phys. Chem. B* **2001**, *105*, 3453−3462.

(29) Deres, A.; Floudas, G. A.; Müllen, K.; Van der Auweraer, M.; De Schryver, F.; Enderlein, J.; Uji-i, H.; Hofkens, J. The Origin of Heterogeneity of Polymer Dynamics near the Glass Temperature As Probed by Defocused Imaging. *Macromolecules* **2011**, *44*, 9703−9709.

(30) Ellison, C. J.; Mundra, M. K.; Torkelson, J. M. Impacts of Polystyrene Molecular Weight and Modification to the Repeat Unit Structure on the Glass Transition−Nanoconfinement Effect and the Cooperativity Length Scale. *Macromolecules* **2005**, *38*, 1767−1778.

(31) DeMaggio, G.; Frieze, W.; Gidley, D.; Zhu, M.; Hristov, H.; Yee, A. Interface and Surface Effects on the Glass Transition in Thin Polystyrene Films. *Phys. Rev. Lett.* **1997**, *78*, 1524−1527.

(32) Molski, A. Statistics of the Bleaching Number and the Bleaching Time in Single-Molecule Fluorescence Spectroscopy. *J. Chem. Phys.* **2001**, *114*, 1142−1147.

(33) Favro, L. D. Theory of the Rotational Brownian Motion of a Free Rigid Body. *Phys. Rev. Lett.* **1960**, *119*, 53−62.

(34) Tao, T. Time-Dependent Fluorescence Depolarization and Brownian Rotational Diffusion Coefficients of Macromolecules. *Biopolymers* **1969**, *8*, 609−632.
(35) Araoz, B.; Täuber, D.; von Borczyskowski, C.; Aramendía, P. F. Cage Effect in Poly(alkyl methacrylate) Thin Films Studied by Nile Red Single Molecule Fluorescence Spectroscopy. *J. Phys. Chem. C* **2012**, *116*, 7573−7580.
(36) The polarized intensities $I_{//}$ and $I_{\perp}$ define the orientation of the projection of the molecular transition dipole moment on the plane of the sample. The resulting in-plane angle α, which we define arbitrarily with respect to the parallel direction, is the only one that can be determined in our experiment. It is related to the anisotropy by: $\tan^2 \alpha = I_{\perp}/I_{//} = (1 - r)/(1 + 2r)$. The operative advantage of using the anisotropy is that its value is restricted to the interval $-0.5 \leq r \leq 1$, whereas $\tan^2 \alpha$ can take any real value.
(37) Suhling, K.; Siegel, J.; Lanigan, P. M.; Lévêque-Fort, S.; Webb, S. E.; Phillips, D.; Davis, D. M.; French, P. M. Time-Resolved Fluorescence Anisotropy Imaging Applied to Live Cells. *Opt. Lett.* **2004**, *29*, 584−586.
(38) Gensch, T.; Böhmer, M.; Aramendía, P. F. Single Molecule Blinking and Photobleaching Separated by Wide-Field Fluorescence Microscopy. *J. Phys. Chem. A* **2005**, *109*, 6652−6658.
(39) *Gaussf*; Delft Image Processing Library. http://www.diplib.org/.
(40) Vallée, R. A.; Rohand, T.; Boens, N.; Dehaen, W.; Hinze, G.; Basché, T. Analysis of the Exponential Character of Single Molecule Rotational Correlation Functions for Large and Small Fluorescence Collection Angles. *J. Chem. Phys.* **2008**, *128*, 154515.
(41) Hellriegel, C.; Kirstein, J.; Bräuchle, C.; Latour, V.; Pigot, T.; Olivier, R.; Lacombe, S.; Brown, R.; Guieu, V.; Payrastre, C.; et al. Diffusion of Single Streptocyanine Molecules in the Nanoporous Network of Sol-Gel Glasses. *J. Phys. Chem. B* **2004**, *108*, 14699−14709.
(42) Krause, S.; Aramendia, P. F.; Täuber, D.; von Borczyskowski, C. Freezing Single Molecule Dynamics on Interfaces and in Polymers. *Phys. Chem. Chem. Phys.* **2011**, *13*, 1754−1761.
(43) Ellison, C. J.; Torkelson, J. M. The Distribution of Glass-Transition Temperatures in Nanoscopically Confined Glass Formers. *Nat. Mater.* **2003**, *2*, 695−700.
(44) Tress, M.; Erber, M.; Mapesa, E. U.; Huth, H.; Müller, J.; Serghei, A.; Schick, C.; Eichhorn, K.-J.; Voit, B.; Kremer, F. Glassy Dynamics and Glass Transition in Thin Polymer Layers of PMMA Deposited on Different Substrates. *Macromolecules* **2010**, *43*, 9937−9944.
(45) Zheng, Z.; Kuang, F.; Zhao, J. Direct Observation of Rotational Motion of Fluorophores Chemically Attached to Polystyrene in Its Thin Films. *Macromolecules* **2010**, *43*, 3165−3168.
(46) Uji-i, H.; Melnikov, S. M.; Deres, A.; Bergamini, G.; De Schryver, F.; Herrmann, A.; Müllen, K.; Enderlein, J.; Hofkens, J. Visualizing Spatial and Temporal Heterogeneity of Single Molecule Rotational Diffusion in a Glassy Polymer by Defocused Wide-Field Imaging. *Polymer* **2006**, *47*, 2511−2518.
(47) Dutt, G. B.; Doraiswamy, S.; Periasamy, N.; Venkataraman, B. Rotational Reorientation Dynamics of Polar Dye Molecular Probes by Picosecond Laser Spectroscopic Technique. *J. Chem. Phys.* **1990**, *93*, 8498−8513.
(48) Eggeling, C.; Widengren, J.; Rigler, R.; Seidel, C. A. M. Photobleaching of Fluorescent Dyes under Conditions Used for Single-Molecule Detection: Evidence of Two-Step Photolysis. *Anal. Chem.* **1998**, *70*, 2651−2659.
(49) Mondal, R.; Shah, B. K.; Neckers, D. C. Determination of Oxygen Permeability of Polymers Using In-Situ Photo-Generated Heptacene. *J. Photochem. Photobiol., A* **2007**, *192*, 36−40.
(50) Kaczmarek, H.; Kaminska, A.; Herk, A. Photooxidative Degradation of Poly (Alkyl Methacrylate)s. *Eur. Polym. J.* **2000**, *36*, 767−777.
(51) Wang, C.-Y.; Ediger, M. D. Lifetime of Spatially Heterogeneous Dynamic Domains in Polystyrene Melts. *J. Chem. Phys.* **2000**, *112*, 6933−6937.